OXFORD

ORIGINAL ARTICLE

Genome-Wide Transcriptional Profiling and Structural Magnetic Resonance Imaging in the Maternal Immune Activation Model of Neurodevelopmental Disorders

Juliet Richetto[1,†], Robert Chesters[2,†], Annamaria Cattaneo[3,4], Marie A. Labouesse[5], Ana Maria Carrillo Gutierrez[2], Tobias C. Wood[6], Alessia Luoni[7], Urs Meyer[1], Anthony Vernon[2,‡], and Marco A. Riva[7,‡]

[1]Institute of Pharmacology and Toxicology, University of Zurich-Vetsuisse, Zurich, Switzerland, [2]Department of Basic and Clinical Neuroscience, Institute of Psychiatry Psychology and Neuroscience, King's College London, London, UK, [3]Biological Psychiatry Laboratory, IRCCS Fatebenefratelli San Giovanni di Dio, Brescia, Italy, [4]Stress, Psychiatry and Immunology Laboratory, Department of Psychological Medicine, Institute of Psychiatry, King's College London, London, UK, [5]Physiology and Behavior Laboratory, ETH Zurich, Schwerzenbach, Switzerland, [6]Department of Neuroimaging, Institute of Psychiatry Psychology and Neuroscience, King's College London, London, UK, and [7]Department of Pharmacological and Biomolecular Sciences, Università degli Studi di Milano, Milan, Italy

Address correspondence to Urs Meyer, Ph.D., Institute of Pharmacology and Toxicology, University of Zurich-Vetsuisse, Winterthurerstrasse 260, 8057 Zurich, Switzerland. E-mail: urs.meyer@vetpharm.uzh.ch

[†]These authors corresponded equally to the present study.

[‡]Shared seniority.

Abstract

Prenatal exposure to maternal infection increases the risk of neurodevelopmental disorders, including schizophrenia and autism. The molecular processes underlying this pathological association, however, are only partially understood. Here, we combined unbiased genome-wide transcriptional profiling with follow-up epigenetic analyses and structural magnetic resonance imaging to explore convergent molecular and neuromorphological alterations in corticostriatal areas of adult offspring exposed to prenatal immune activation. Genome-wide transcriptional profiling revealed that prenatal immune activation caused a differential expression of 116 and 251 genes in the medial prefrontal cortex and nucleus accumbens, respectively. A large part of genes that were commonly affected in both brain areas were related to myelin functionality and stability. Subsequent epigenetic analyses indicated that altered DNA methylation of promoter regions might contribute to the differential expression of myelin-related genes. Quantitative relaxometry comparing T_1, T_2, and myelin water fraction revealed sparse increases in T_1 relaxation times and consistent reductions in T_2 relaxation times. Together, our multi-system approach demonstrates that prenatal viral-like immune activation causes myelin-related transcriptional and epigenetic changes in corticostriatal areas. Even though these abnormalities do not seem to be associated with overt white

matter reduction, they may provide a molecular mechanism whereby prenatal infection can impair myelin functionality and stability.

Introduction

The etiology of multifactorial and multi-symptomatic neuropsychiatric disorders likely includes exposures to adverse events during prenatal and early postnatal life, which may disrupt the development and maturation of neural systems and brain functions (Brown 2011). Prenatal exposure to infectious or inflammatory insults is increasingly recognized to play an important role in this context. Indeed, immune-related prenatal adversities have been repeatedly linked with a higher risk of neurodevelopmental psychiatric disorders, including schizophrenia, autism, and bipolar disorder (Brown and Derkits 2010; Patterson 2011; Marangoni et al. 2016). These epidemiological associations are further supported by translational work in animal models demonstrating abnormal brain development and behavioral dysfunctions following prenatal administration of infectious pathogens or immune activating agents (Meyer and Feldon 2010; Harvey and Boksa 2012; Meyer 2014).

The advances in modeling prenatal immune activation effects in animals hold promise for the identification of pathological mechanisms that translate the prenatal insult into long-term brain abnormalities. The majority of these experimental attempts, however, were hypothesis-driven and focused on the role of a specific cellular or molecular mechanism, pathway or system (Eyles et al. 2012; Ibi and Yamada 2015). While this is a laudable and possibly fruitful approach for the examination of a presumed pathophysiological process, hypothesis-driven investigations may mask the discovery of novel disease mechanisms.

The implementation of genome-wide transcriptional profiling is one possible strategy to overcome these limitations. It allows an unbiased screen of gene expression changes in response to prenatal immune activation, which can form the basis for follow-up investigations that take into account this transcriptomic information (Fatemi et al. 2005, 2008, 2009a; Connor et al. 2012; Tebbenkamp et al. 2014; Horvath and Mirnics 2015). The present study followed such an approach, in which unbiased transcriptomic profiling formed the basis for subsequent immunohistochemical investigations and epigenetic analyses. Genome-wide transcriptomic profiling was performed using unbiased microarray techniques in the medial prefrontal cortex (mPFC) and nucleus accumbens (NAc), 2 brain regions implicated in neurodevelopmental disorders such as schizophrenia and autism (Richey et al. 2015; Schubert et al. 2015; Selemon and Zecevic 2015). The inclusion of 2 brain regions allowed us to identify region-specific and -overlapping transcriptomic effects of prenatal immune activation using a within-subjects comparison. These investigations were performed in offspring that were first subjected to behavioral and cognitive testing.

We also explored whether microscale molecular alterations reverberate to influence macroscale features that are detectable using clinically comparable magnetic resonance imaging (MRI) (Turkheimer et al. 2015). As an adjunct to cellular and molecular methods, MRI provides a non-invasive global visualization of brain maturation, through the evolution of gray and white matter contrast on T_1 and T_2 relaxation time-weighted images (Ballesteros et al. 1993; Paus et al. 2001; Leppert et al. 2009). We further implemented a novel multicomponent relaxation (MCR) technique termed multicomponent-driven equilibrium single pulse observation of T_1 and T_2 (mcDESPOT) (Deoni et al. 2008a) to provide quantitative information about proton tissue water relaxation times and myelin water fraction (MWF) signals. This technique aims to divide the MR signal resulting from steady-state sequences into 3 pools representing water trapped in the myelin sheath, intra-extracellular water, and free water in cerebrospinal fluid (Deoni et al. 2008b, 2013). Whilst applied in human imaging before (Deoni et al. 2011, 2012), we have recently validated the mcDESPOT methodology in rodents using a model of cuprizone-induced demyelination (Wood et al. 2016a, 2016b).

All investigations were performed using a well-established mouse model of prenatal viral-like immune activation. The model is based on maternal administration of the viral mimetic poly(I:C) (=*polyriboinosinic-polyribocytidilic acid*), which induces a cytokine-associated viral-like acute phase response in maternal and fetal compartments, including the fetal brain (Meyer et al. 2009). Prenatal poly(I:C) treatment in rodents has repeatedly been shown to cause multiple behavioral and cognitive disturbances in the offspring, many of which are implicated in developmental psychiatric disorders such as schizophrenia and autism (Meyer et al. 2009; Meyer and Feldon 2010; Harvey and Boksa 2012; Meyer 2014). The poly(I:C) administration model thus offers a unique opportunity to explore genome-wide transcriptomic changes following prenatal exposure to an etiologically relevant risk factor, and to further link such changes with neurobehavioral and MRI-detectable abnormalities.

Materials and Methods

Animals

C57Bl6/N mice were used throughout the study. Female and male mice were originally obtained from Charles River Laboratories (Germany) and kept in our in-house specific-pathogen-free (SPF) facility until breeding began to generate poly(I:C)-exposed and control offspring (see below). All animal breeding and holding rooms were temperature- and humidity-controlled (21 $\pm$ 1°C, 55 $\pm$ 5%) and kept under a reversed light–dark cycle (lights off: 7:00 A.M. to 7:00 P.M.). All animals had ad libitum access to food (Kliba 3430, Kaiseraugst, Switzerland) and water throughout the entire study. All procedures described in the present study had been previously approved by the Cantonal Veterinarian's Office of Zurich, and all efforts were made to minimize the number of animals used and their suffering.

Maternal Immune Activation during Pregnancy

Female C57Bl6/N mice were subjected to a timed mating procedure as described previously (Meyer et al. 2005). Pregnant dams on gestation day (GD) 17 were randomly assigned to receiving either a single injection of poly(I:C) (potassium salt; Sigma-Aldrich, Buchs, St Gallen, Switzerland) or vehicle. Poly(I:C) (5 mg/kg; calculated based on the pure form of poly(I:C)) was dissolved in sterile pyrogen-free 0.9% NaCl (vehicle) solution to yield a final concentration of 1 mg/mL and was administered intravenously (i.v.) into the tail vein under mild physical constraint. The dose of poly(I:C)

was selected based on previous dose–response studies (Meyer et al. 2005). 10 pregnant dams were injected with poly(I:C), and another 10 with vehicle solution.

GD 17 in the mouse roughly corresponds to human gestational weeks 28 to 29 in terms of cortical neurogenesis (http://translatingtime.net/translate). It was selected based on previous studies showing that prenatal poly(I:C) exposure during this gestational period causes adult behavioral, cognitive, and neuroanatomical abnormalities relevant to neurodevelopmental brain disorders, including schizophrenia and autism (Meyer et al. 2006, 2008; Bitanihirwe et al. 2010a, 2010b; Richetto et al. 2013, 2014, 2015). We previously verified that poly(I:C) administration on GD 17 is effective in terms of eliciting cytokine-associated inflammatory response in maternal and fetal tissues (Meyer et al. 2006).

Allocation of Offspring and Group Sizes

Offspring of poly(I:C)-treated dams (POL) and vehicle-exposed control offspring (CON) were weaned and sexed on postnatal day (PND) 21. Littermates of the same sex were caged separately and maintained in groups of 3 to 4 animals per cage. Only male animals were included in all experiments because our previous research using the mouse prenatal poly(I:C) administration model did not reveal sex-dependent effects on the behavioral and cognitive functions of primary interest, including social interaction and working memory (Meyer et al. 2008; Bitanihirwe et al. 2010a; Richetto et al. 2013). A first cohort of CON and POL offspring was used for the assessment of behavioral and cognitive functions, which was followed by *postmortem* microarray analyses, validation of gene expression, and DNA methylation analyses (see below). A second cohort of offspring was used for *ex vivo* MRI imaging and subsequent *postmortem* immunohistochemical analyses (see below). In both cohorts, 1 male offspring per litter was randomly selected for the investigations of interest in order to avoid litter effects (Zorrilla 1997). This led to a group size of $N = 10$ offspring per prenatal treatment condition in each cohort. The DNA methylation analyses were performed using a subset of offspring, with $N = 5$ offspring per prenatal treatment condition. A graphical representation of the experimental design is provided in Supplementary Figure 1.

Behavioral Testing

CON and POL offspring of cohort 1 were subjected to cognitive and behavioral testing when they reached early adulthood (12 weeks of age). The tests included paradigms assessing social approach behavior, and social recognition, and short-term spatial recognition memory working. These tests were selected based on their relevance to neurodevelopmental disorders with infectious and inflammatory components, including schizophrenia and autism (Meyer et al. 2009; Peleg-Raibstein et al. 2012). A detailed description of the test apparatuses and procedures is provided in the Supplementary Information. Each animal underwent all behavioral tests in the following order: (1) spatial recognition memory test and (2) social approach and recognition test. A test-free resting period of 2 days was imposed between the 2 tests.

Collection of Brain Samples for Molecular Analyses

CON and POL offspring of cohort 1 were killed by decapitation 10 days after completion of behavioral testing for the subsequent molecular analyses. The brains were rapidly extracted from the skull (within < 20 s) and placed on an ice-chilled plate. This was followed by preparing 1-mm coronal brain sections using razorblade cuts and subsequent micro-dissection of the brain areas of interest. We dissected the medial prefrontal cortex (mPFC, including anterior cingulate, prelimbic and dorsal parts of the infralimbic cortices; bregma: +2.3 to +1.3 mm) and the nucleus accumbens (NAc, including core and shell subregions; bregma +1.5 to +0.5 mm) as previously described (Bitanihirwe et al. 2010a). Brain specimens were collected in 96-well microtiter plates kept on dry ice and allowed to freeze before storage at −80°C until further use.

DNA and RNA Isolation

Total DNA and RNA were isolated using the Qiagen AllPrep DNA and RNA Mini kit (Qiagen, Italy) as described in the Supplementary Information.

Microarray Analyses

Genome-wide gene expression analyses were performed using Affymetrix microarray assays (Mouse Gene 1.1 ST Array Strips on GeneAtlas platform), following the 3'IVT one cycle labeling as fully described in the Supplementary Information. All the raw data are accessible at the NCBI GEO depository (GEO accession number GSE77973). The data analysis was performed with Partek Genomics Suite (Partek, USA), version 6.6 (for details, see Supplementary information). Differentially expressed genes (DEGs) in POL offspring relative to CON offspring were identified by performing a linear contrast (POL versus CON). In this comparison, a maximum filter of $P < 0.05$ and a minimum absolute fold change cut-off of 1.2 were applied. The DEGs were loaded into Partek Genomics Suite and were clustered according to the Hierarchical Clustering function of Partek Genomics Suite. For this purpose, the data was normalized with standardization (each column mean is 0, and the standard deviation is scaled to 1), and then multidimensional scaling with a Euclidian distance metric was performed on the normalized samples to allow visualization of the distance between them. To confirm that the overlapping changes were not due to random distribution, we performed the hyper-geometric test in R ($P = 5.765284e14$). Gene Ontology enrichment analyses were performed using Partek Genomics Suite (Partek, USA). Subsequent validation of selected DEGs was performed by quantitative real-time PCR as described below.

Quantitative Real-Time RT-PCR Analyses

mRNA levels were quantified by TaqMan qRT-PCR (CFX384 real-time system, Bio-Rad Laboratories) using the iScript 1-step RT-PCR kit for probes (Bio-Rad Laboratories) (see Supplementary Information). Relative target gene expression was calculated according to the 2(-Delta Delta C(T)) method. Probe and primer sequences of Claudin11 (Assay: Mm00500915_m1) were purchased from Life Technologies (Switzerland), while the custom designed probe and primer sequences used for MOBP, MOG, MAL and MAG are summarized in Supplementary Table 1 and were purchased from Eurofins Genomics GmbH (Germany).

DNA Methylation Analysis

DNA methylation levels of the α-myelin-associated oligodendrocytic basic protein (MOBP) promoter region were quantified using the EpiTYPER assay. This technique detects and quantifies DNA methylation using base-specific cleavage and Matrix-Assisted Laser Desorption/Ionization Time-of-Flight (MALDI-TOF) mass

spectrometry (Suchiman et al. 2015). Genomic DNA was treated and analysed as fully described in the Supplementary Information.

Brain Sample Preparation for MRI

At 12 weeks of age, CON and POL offspring from the second cohort were deeply anaesthetized with an overdose of Nembutal (Abbott Laboratories) and perfused transcardially with 0.9% NaCl, followed by 4% phosphate-buffered paraformaldehyde (PFA) solution containing 15% picric acid (Giovanoli et al. 2013). After perfusion, the animals were decapitated and the skin, lower jaw and ears were removed. The brain within the skull was incubated in 4% PFA overnight at +4°C and then shipped to King's College London the next day. Upon arrival, brain samples were transferred to 0.01 M phosphate-buffered saline containing and 0.05% sodium azide for at least 7 days prior to MR imaging.

MRI acquisition, Processing and Analysis

A 7 T horizontal small bore magnet and (Agilent Technologies Inc. Santa Clara, USA) and a quadrature volume radiofrequency coil (39 mm internal diameter, Rapid Biomedical GmbH) were used for all MRI acquisitions. Fixed brain samples were placed securely up to 4 at a time in an MR-compatible holder and immersed in proton-free susceptibility matching fluid (Fluorinert^{TM} FC-70; Sigma-Aldrich, UK). The following MR images were acquired: T_2-weighted 3D Fast Spin-Echo (FSE) and a multicomponent Driven Equilibrium Single Pulse Observation of T_1 and T_2 (mcDESPOT) protocol with B1 correction. The latter consists of a Spoiled Gradient echo (SPGR), balanced Steady State Free Procession (bSSFP) and Actual Flip-angle imaging (AFI) scans (Deoni et al. 2013). The mcDESPOT protocol generates data to calculate parametric maps of T_1, T_2, and the myelin water fraction (MWF) for each animal (Supplementary Figure 1). Parameters for each scan are summarized in Supplementary Table 3. MR image processing and analysis were performed as fully described in the Supplementary information.

Group-level differences in MRI parameters (volume, T_1, T_2, and MWF) between CON and POL offspring were analysed voxel-wise across the whole-brain using permutation testing and threshold free cluster enhancement (TFCE) implemented in FSL Randomize (Smith and Nichols 2009) and corrected for multiple comparisons using the false discovery rate (FDR) (Genovese et al. 2002) at $q = 0.05$. For volume, comparisons were made between CON ($N = 10$) and POL ($N = 10$) offspring. For mcDESPOT data, comparisons were made between CON ($N = 6$) and POL ($N = 8$) offspring, as 4 scans from the CON group and 2 scans from the POL group had to be discarded due to artefacts in the data (see Supplementary Information).

Immunohistochemistry

After completion of all MRI, fixed brain tissues were processed for immunohistochemical analyses as described in the Supplementary information. Standard immunohistochemical procedures were implemented to stain for α-myelin basic protein (MBP; rabbit anti-MBP; Abcam, Cat no. ab7349; diluted 1:1000) and MOBP (rabbit anti-MOBP; Abcam, Cat no. ab203388; diluted 1:500) as fully described in the Supplementary information.

Threshold Image Analysis for Myelin Staining

Quantitative analyses of MBP and MOBP-positive staining were performed in the mPFC using unbiased threshold image analysis as described in the Supplementary Information. All post-processing and analysis was performed using ImageJ software (http://imagej.nih.gov/ij/). The percentage area of immunopositive pixels in each acquired image of the mPFC, from 4 consecutive sections, were averaged to give a single value per animal.

Statistical Analyses

All behavioral and RT-PCR were analysed using independent Student's t-tests (2-tailed). Immunohistochemical analysis was conducted using a 1-tailed Student's T-test, given the a-priori hypothesis based on the strong gene expression data. Statistical significance was set at $P < 0.05$ for these analyses. Microarray and MRI data were analysed as described above. DNA methylation levels measured using EpiTYPER were analysed using repeated-measures analysis of variance (RM-ANOVA) followed by Fisher's least significant difference (FLSD) post hoc comparisons whenever appropriate. Correlative analyses between the dependent measures of primary interest (behavioral and cognitive data, mRNA and DNA methylation data, MRI data, and immunohistochemical data) were performed using first-order partial correlations partialling for the 2 prenatal treatment conditions. Hence, partial correlations were used to control for the effects of the independent variable "prenatal immune activation". All statistical analyses were performed using the statistical software SPSS (v22.0; IBM Corporation, Armonk, New York, USA).

Results

Prenatal immune activation induces deficits in short-term spatial recognition memory and social interaction

First, we aimed to ascertain the effects of prenatal immune activation on adult behavioral and cognitive functions. We found that POL offspring displayed impaired performance in a Y-maze spatial recognition memory test. (Fig. 1A). In this test, the critical measure of spatial recognition memory is the relative time spent in the novel (previously unexplored) arm during the choice phase. CON offspring displayed a noticeable preference towards the novel arm, indicating intact spatial recognition memory in these groups (Fig. 1A). In contrast, POL offspring exhibited a marked reduction ($P < 0.05$) in this measure and performed only at chance level (Fig. 1A). There were no group differences with respect to the total distance moved (Fig. 1A), indicating that the negative effects of prenatal immune activation on spatial recognition memory are not confounded by possible differences in basal locomotor activity.

POL offspring also displayed impaired marked deficits in the social interaction test, in which they were first allowed to concomitantly explore an inanimate dummy object and an unfamiliar live mouse (Fig. 1B). During this phase of the test, CON offspring showed a clear preference (>65%) for the live mouse versus the inanimate dummy object (Fig. 1B). By contrast, POL offspring did not display such a preference (Fig. 1B), indicating reduced sociability towards unfamiliar conspecifics. This led to a significant ($P < 0.001$) group difference in the percent time spent with the live mouse (Fig. 1B).

To test social recognition memory, the inanimate dummy object was then replaced by another unfamiliar live mouse, and the relative exploration time between the previously explored and novel live mouse was measured. During this phase of the social interaction test, CON offspring showed a clear preference (>65%) for the novel mouse (Fig. 1B). POL offspring did not
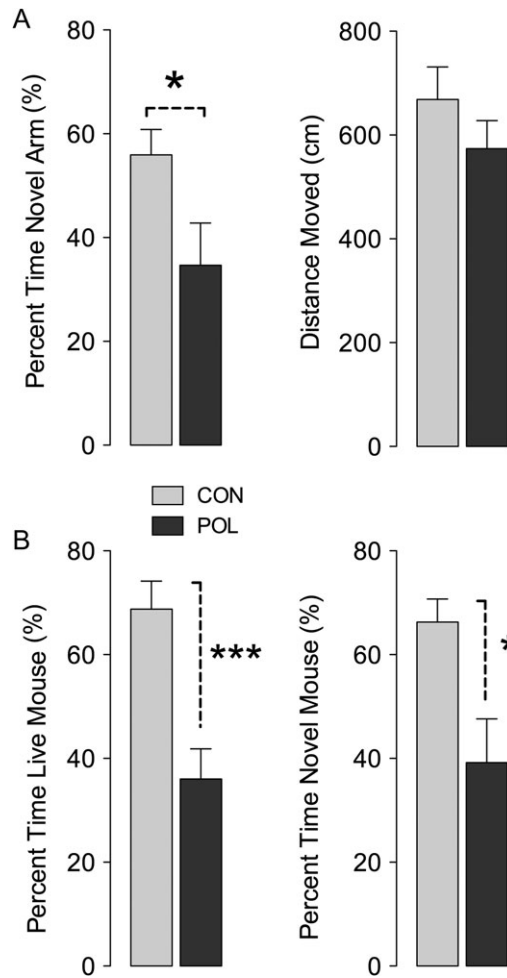
Figure 1. Cognitive and behavioral deficits following late prenatal immune activation. Mice were subjected to prenatal poly(I:C) treatment on gestation day 17 (POL), or they were exposed to prenatal control (CON) treatment. **(A)** Percent time spent in the novel arm during the Y-maze working memory test. *$P < 0.05$ based on independent Student's t tests (2-tailed). **(B)** Percent time spent with an unfamiliar live mouse, relative to an inanimate dummy object, during the social interaction test; and percent time spent with a novel live mouse, relative to a familiar one, during the social recognition test. *$P < 0.05$ and ***$P < 0.001$ based on independent Student's t tests (2-tailed). All data are based on N (CON) = 10, N(POL) = 10 and represent means ± s.e.m.

Figure 2. Unique and common gene expression differences following late prenatal immune activation in the mPFC and NAc, revealed by microarray. Mice were subjected to prenatal poly(I:C) treatment on gestation day 17 (POL), or they were exposed to prenatal control (CON) treatment. **(A)** Hierarchical clustering of differentially expressed genes in POL offspring relative to CON offspring in the mPFC and NAc. Down- and upregulated genes are represented in purple and yellow color, respectively. **(B)** Venn Diagram depicting the number of genes that are uniquely and commonly affected in the mPFC and NAc of POL offspring. The commonly affected genes are listed for each brain area, with down- and upregulated genes being represented by blue and red color, respectively. All data are based on N(CON) = 6, N(POL) = 6.

display such a preference, leading to a significant ($P < 0.05$) group difference in the percent time spent with the novel mouse (Fig. 1B). In both phases of the social interaction test, there were no group differences with respect to the total distance moved. Hence, prenatal immune activation leads to genuine deficits in social approach behavior and short-term spatial recognition memory without concomitant effects on general exploratory behavior.

Prenatal immune activation alters the long-term transcription profile of the medial prefrontal cortex and nucleus accumbens

As shown in Figure 2A, which represents the hierarchical clustering of expression changes induced by prenatal infection with poly(I:C), 116 genes were differentially expressed in the mPFC (fold change cut-off: ± 1.2; $P < 0.05$), while 251 were differentially expressed in the NAc. Of the 116 genes that were differentially
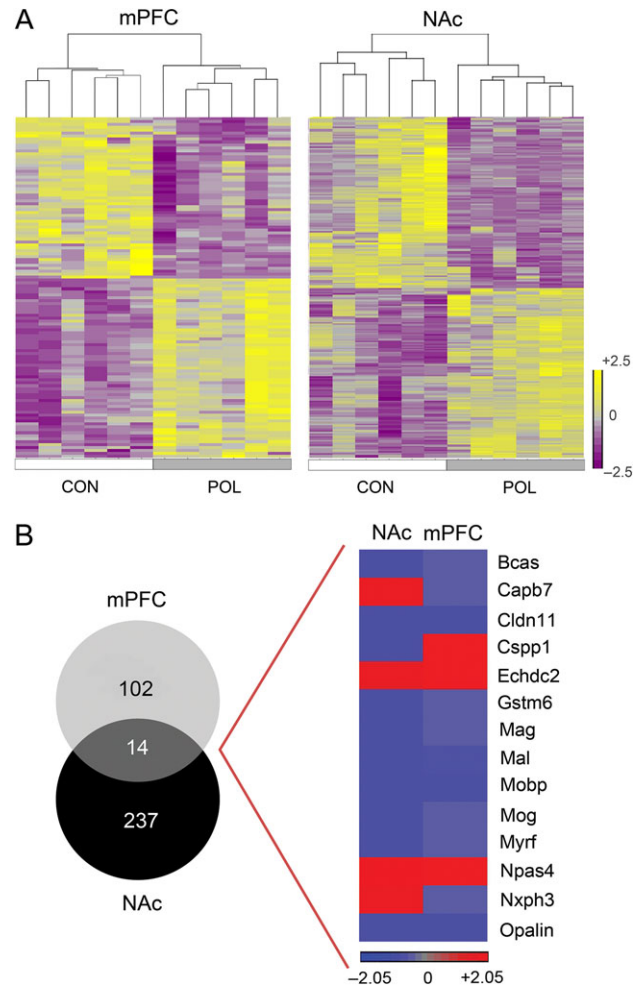
expressed in the mPFC, 55 were downregulated and 61 were upregulated (Tables 1 and 2), while in the NAc, 126 were downregulated and 125 upregulated (Tables 3 and 4). Interestingly, many of these have been already associated with schizophrenia, such as adenosine 2a receptor (ADORA2a), apolipoprotein D (APOD), the dopamine receptors DRD2 and DRD3, forkhead box P2 (FOXP2), glutaminase (GLS), the glutamate receptor subunit GRIN2A, histone cluster 1 (HIST1H2BC), 5-hydroxytryptamine receptors (HTR1A, HTR2A, HTR4), oxytocin (OXT), solute carriers (SLC17A7), and, among others, vesicle-associated membrane protein 4 (VAMP4) (Butler et al. 2016). A Gene Ontology (GO) enrichment analysis computing the DEGs in the mPFC and NAc is presented in Supplementary Table 2.

Next, the genes affected in both brain areas were compared. As shown in Figure 2B, the Venn diagram of the 2 brain areas highlighted 14 common genes, 11 of which are modulated in the same direction in both brain areas (Fig. 2B). In particular,

Table 1 The table represents the 55 downregulated genes in the mPFC as revealed by microarray. All data are based on N(CON) = 6, N(POL) = 6

Gene	Fold change	P-value
Adamts4	−1.259	0.00291
Adora2a	−1.260	0.02701
Adra2a	−1.222	0.01440
Bcas1	−1.242	0.00095
Cabp7	−1.232	0.03128
Cdca7	−1.225	0.00062
Cldn11	−1.356	0.00088
Clic4	−1.216	0.00030
Cnp	−1.265	0.00317
Cpm	−1.215	0.00897
Cryge	−1.657	0.04590
Cyp2j12	−1.215	0.00246
Cyp4a28-ps	−1.330	0.00077
Dlk1	−1.215	0.03507
Dnali1	−1.205	0.00218
Drd2	−1.453	0.03478
Fa2h	−1.297	0.01749
Galnt6	−1.259	0.00046
Gas5	−1.721	0.00002
Glp1r	−1.360	0.02303
Gpr6	−1.405	0.01594
Gstm6	−1.241	0.01346
Hist1h2bb	−1.269	0.00025
Hist1h2bq	−1.202	0.00064
Lrrc10b	−1.273	0.00186
Mag	−1.261	0.01173
Mal	−1.312	0.00395
Mobp	−1.417	0.00124
Mog	−1.250	0.02082
mt-Ta	−3.146	0.00019
mt-Tq	−1.253	0.02654
mt-Tv	−1.322	0.01354
Myrf	−1.229	0.00307
Nnat	−1.266	0.00510
Nxph3	−1.211	0.02714
Opalin	−1.333	0.02207
Pcp4l1	−1.204	0.02124
Ppp1r1b	−1.205	0.00369
Prelp	−1.209	0.01465
Rem2	−1.203	0.00109
Rny1	−1.558	0.00612
Rpl7a	−1.207	0.00078
Rps27rt	−1.206	0.00008
Rybp	−1.205	0.00002
Sf3b4	−1.234	0.01561
Shisa6	−1.216	0.00798
Sox4	−1.231	0.00129
Thbs4	−1.455	0.00133
Trf	−1.235	0.00786
Tspan2	−1.236	0.00875
Txnip	−1.210	0.04400
Ube2v1	−1.237	0.00744
Ugt8a	−1.203	0.02783
Zcchc12	−1.213	0.01511
Zic1	−1.301	0.03720

Table 2 The table lists the 61 upregulated genes in the mPFC as revealed by microarray. All data are based on N(CON) = 6, N(POL) = 6

Gene	Fold change	P-value
Aak1	1.212	0.00227
Adamts10	1.217	0.00008
Atp11b	1.300	0.00070
BC005561	1.221	0.00146
BC030499	1.493	0.00080
Cdh12	1.218	0.00004
Chuk	1.202	0.00032
Coro6	1.318	0.00003
Cpne9	1.223	0.00090
Cspp1	1.234	0.00005
Ddx26b	1.267	0.00126
Dnajc13	1.212	0.00141
Echdc2	1.238	0.01081
Eif2s3y	1.446	0.02942
Eml5	1.234	0.00236
Fam178a	1.236	0.00081
Fat3	1.276	0.00084
Fcf1	1.209	0.00307
Firre	1.204	0.04499
Flnb	1.221	0.00683
Gpatch8	1.287	0.00472
Gtf3c2	1.209	0.01987
Herc6	1.244	0.00051
Hnrnpu	1.463	0.00304
Kansl1	1.348	0.01338
Leng8	1.372	0.00557
Luc7l3	1.220	0.00244
Malat1	1.343	0.01141
Meg3	1.312	0.00568
Mirg	1.398	0.00012
mt-Ty	1.251	0.00880
Myo9a	1.244	0.00058
Npas4	1.587	0.01846
Nup93	1.239	0.00071
Nvl	1.246	0.00027
Paxbp1	1.225	0.00141
Phf20l1	1.232	0.01339
Pisd-ps1	1.240	0.02393
Pisd-ps2	1.206	0.00064
Pnet-ps	1.290	0.01531
Pnisr	1.332	0.00103
Prpf39	1.299	0.00094
Rbm12b2	1.238	0.00561
Rbm33	1.318	0.00284
Rnpc3	1.321	0.00096
Rps6kb2	1.225	0.00088
Rxfp1	1.211	0.00002
Sfswap	1.218	0.00018
Slc9b2	1.221	0.00003
Smpd4	1.262	0.00036
Snhg11	1.269	0.00258
Taf1d	1.228	0.00118
Tfrc	1.205	0.00033
Tmem181a	1.246	0.00040
Trank1	1.340	0.00047
Ttc14	1.364	0.00064
Uggt2	1.381	0.00061
Vmn2r84	1.307	0.00099
Vmn2r86	1.578	0.00221
Wsb1	1.243	0.00812
Zcchc7	1.235	0.00203

poly(I:C) exposure affected the expression of 6 main genes involved in myelination, both in the mPFC and in the NAc: myelin and lymphocyte protein (MAL), myelin-associated glycoprotein (MAG), myelin-associated oligodendrocytic basic

Table 3 The table lists the 126 downregulated genes in the NAc as revealed by microarray. All data are based on N(CON) = 6, N(POL) = 6

Gene	Fold change	P-value
Agt	−1.733	0.0412
Ankub1	−1.333	0.0261
Anln	−1.293	0.0299
Apod	−1.226	0.0014
Arhgdib	−1.300	0.0182
Arsg	−1.248	0.0006
Aspa	−1.352	0.0117
Atp13a4	−1.210	0.0284
BC005624	−1.204	0.0000
Bcas1	−1.250	0.0009
Cacng4	−1.226	0.0154
Calml4	−1.267	0.0372
Capsl	−1.353	0.0452
Ccdc170	−1.222	0.0401
Cd63	−1.298	0.0066
Cd82	−1.343	0.0055
Cdhr3	−1.379	0.0424
Chd6	−1.207	0.0247
Chd7	−1.215	0.0308
Cldn10	−1.213	0.0073
Cldn11	−1.227	0.0028
Clmn	−1.243	0.0309
Cobl	−1.216	0.0254
Coch	−1.378	0.0081
Crabp1	−1.296	0.0034
Cspp1	−1.255	0.0247
Ctnna1	−1.221	0.0016
Cyp2j9	−1.270	0.0019
Dnah3	−1.358	0.0258
Ebf1	−1.330	0.0005
Ebf2	−1.267	0.0446
Ebf3	−1.321	0.0181
Edil3	−1.210	0.0134
Eif3e	−1.250	0.0011
Elovl7	−1.343	0.0338
Enpp2	−1.691	0.0318
Ephx1	−1.209	0.0028
Evi2a	−1.246	0.0064
Fmo1	−1.219	0.0106
Frem3	−1.213	0.0017
Gab1	−1.210	0.0021
Gal	−2.353	0.0002
Galr1	−1.307	0.0126
Glis3	−1.255	0.0121
Gpr37	−1.293	0.0084
Gstm6	−1.225	0.0242
Hist1h1c	−1.409	0.0002
Hist1h2bc	−1.265	0.0036
Hmcn1	−1.236	0.0018
Iqcg	−1.300	0.0422
Iqcj	−1.209	0.0017
Itpkb	−1.270	0.0449
Kif6	−1.206	0.0040
Mag	−1.241	0.0223
Mal	−1.318	0.0013
Meig1	−1.416	0.0274
Mgst1	−1.266	0.0023
Mobp	−1.423	0.0000
Mog	−1.263	0.0121
Mpeg1	−1.293	0.0007
mt-Tf	−1.233	0.0018

(Continued)

Table 3 (Continued)

Gene	Fold change	P-value
mt-Tn	−1.591	0.0033
Mtx2	−1.209	0.0123
Myrf	−1.313	0.0009
Ndrg1	−1.237	0.0083
Nhp2	−1.331	0.0112
Nme5	−1.241	0.0096
Nr2f2	−1.698	0.0014
Nsmce4a	−1.232	0.0010
Opalin	−1.480	0.0015
Oxt	−1.322	0.0018
Pcolce2	−1.338	0.0081
Pde8a	−1.223	0.0056
Phldb1	−1.247	0.0013
Pigk	−1.203	0.0018
Pir	−1.218	0.0032
Pld1	−1.210	0.0284
Pllp	−1.301	0.0011
Prlr	−2.081	0.0194
Prox1	−1.400	0.0171
Prr18	−1.224	0.0049
Prrg4	−1.267	0.0325
Psma1	−1.200	0.0039
Rarres2	−1.234	0.0476
Rassf2	−1.270	0.0008
Rdm1	−1.675	0.0130
Rgs10	−1.238	0.0101
Rgs3	−1.292	0.0011
Ror1	−1.233	0.0250
Rpl26	−1.264	0.0036
Rpl35a	−1.212	0.0126
Rpl36	−1.203	0.0054
S1pr5	−1.252	0.0037
Scarna13	−1.446	0.0097
Sccpdh	−1.275	0.0102
Sgms2	−1.253	0.0221
Shank2	−1.478	0.0088
Slirp	−1.269	0.0115
Smco3	−1.234	0.0137
Sorcs1	−1.228	0.0014
Sparc	−1.289	0.0360
Spef2	−1.474	0.0195
St6galnac1	−1.222	0.0006
Stxbp3a	−1.258	0.0001
Synpo2	−1.308	0.0016
Tac2	−2.333	0.0005
Tcf7l2	−1.341	0.0309
Tcn2	−1.223	0.0208
Tm4sf1	−1.225	0.0454
Tmbim1	−1.235	0.0033
Tmem212	−1.250	0.0335
Tmem215	−1.215	0.0010
Tnfaip6	−1.236	0.0133
Trdn	−1.242	0.0017
Trh	−1.303	0.0038
Ttc21a	−1.221	0.0254
Ttr	−7.075	0.0118
Unc13c	−1.275	0.0141
Vamp4	−1.315	0.0003
Vps4b	−1.219	0.0005
Wdr49	−1.286	0.0091
Wdr63	−1.205	0.0120

(Continued)

Table 3 (Continued)

Gene	Fold change	P-value
Wdr96	−1.228	0.0156
Whrn	−1.278	0.0360
Zbtb10	−1.209	0.0080
Zfhx3	−1.217	0.0384

Table 4 The table lists the 125 upregulated genes in the NAc as revealed by microarray. All data are based on N(CON) = 6, N(POL) = 6

Gene	Fold change	P-value
Adamts3	1.325	0.0018
Adat3	1.235	0.0168
Adh5	1.202	0.0049
Ahr	1.234	0.0005
Ankrd45	1.275	0.0001
Apbb3	1.215	0.0003
Arpc5	1.206	0.0437
Azin1	1.288	0.0002
B3galt2	1.443	0.0164
Bcl11a	1.203	0.0393
Bmp3	1.292	0.0488
Brinp2	1.225	0.0127
Btbd3	1.238	0.0163
Cabp7	1.270	0.0108
Cacna2d1	1.325	0.0091
Cacnb3	1.210	0.0270
Cckbr	1.371	0.0399
Cecr6	1.226	0.0433
Clec2l	1.226	0.0088
Cnih3	1.455	0.0174
Cntnap3	1.270	0.0394
Col6a1	1.329	0.0023
Crebbp	1.201	0.0001
Csgalnact1	1.325	0.0034
Ctgf	1.664	0.0466
Dab1	1.221	0.0143
Dclk3	1.218	0.0219
Dkk3	1.216	0.0188
Drd3	1.507	0.0005
Dsg1a	1.277	0.0003
Dsg1c	1.242	0.0012
Echdc2	1.200	0.0246
Eri2	1.293	0.0148
Fam131a	1.388	0.0041
Fgf10	1.230	0.0139
Foxp2	1.215	0.0144
Galnt9	1.326	0.0261
Gls	1.287	0.0120
Gnrh1	1.272	0.0243
Gpr126	1.277	0.0066
Gpr149	1.284	0.0203
Gpr26	1.355	0.0138
Grin2a	1.262	0.0381
Gtpbp2	1.204	0.0003
Gtpbp8	1.322	0.0397
Hmgcr	1.215	0.0216
Hsd17b7	1.262	0.0254
Hspbp1	1.233	0.0250
Htr1a	1.387	0.0264
Htr2a	1.360	0.0410
Htr4	1.316	0.0019

(Continued)

Table 4 (Continued)

Gene	Fold change	P-value
Igsf21	1.322	0.0290
Islr2	1.319	0.0137
Itpka	1.231	0.0086
Kcnab3	1.251	0.0096
Kcnh3	1.232	0.0390
Kctd16	1.247	0.0410
Kifc2	1.231	0.0029
Lix1	1.270	0.0084
Lmo4	1.201	0.0011
Lrrc55	1.318	0.0065
Mafg	1.205	0.0026
Mef2c	1.304	0.0214
Mef2d	1.287	0.0040
Mgll	1.267	0.0019
Morn4	1.201	0.0087
Mpped1	1.331	0.0295
Myo16	1.345	0.0017
Napb	1.232	0.0460
Ndnf	1.341	0.0403
Ndufa13	1.201	0.0015
Nmbr	1.776	0.0373
Nov	2.691	0.0160
Npas4	1.574	0.0214
Nptx1	1.645	0.0140
Npy1r	1.303	0.0316
Ntn1	1.291	0.0062
Nxph3	1.302	0.0295
Ociad2	1.265	0.0208
Olfm3	1.248	0.0229
Pbrm1	1.228	0.0279
Pcsk5	1.229	0.0020
Pdcd4	1.213	0.0236
Pde1a	1.341	0.0028
Pdyn	1.251	0.0358
Pls3	1.211	0.0446
Pou3f4	1.201	0.0369
Ppp1r12b	1.234	0.0074
Prr14l	1.238	0.0214
Rap1gap2	1.207	0.0301
Rapgefl1	1.337	0.0103
Rasl10b	1.215	0.0222
Rfk	1.237	0.0258
Rnf26	1.217	0.0257
Rnf39	1.267	0.0059
Satb1	1.274	0.0366
Sema5b	1.235	0.0107
Sidt1	1.432	0.0278
Slc17a7	2.840	0.0490
Slc2a3	1.242	0.0018
Slc7a4	1.224	0.0016
Slco5a1	1.234	0.0030
Slit2	1.279	0.0420
Sprn	1.263	0.0206
Spryd3	1.205	0.0266
St3gal1	1.619	0.0005
Stard5	1.685	0.0063
Stra6	1.396	0.0103
Strip2	1.239	0.0427
Sult4a1	1.299	0.0106
Svop	1.232	0.0070
Szt2	1.283	0.0013

(Continued)

Table 4 (Continued)

Gene	Fold change	P-value
Tenm4	1.233	0.0027
Tmem132d	1.205	0.0456
Tmem160	1.317	0.0015
Tmem56	1.206	0.0439
Tpbg	1.215	0.0085
Trim23	1.254	0.0175
Tsnax	1.245	0.0001
Ttc39b	1.234	0.0325
Ube3b	1.224	0.0018
Uck2	1.220	0.0160
Uqcrc1	1.251	0.0000
Wdr54	1.258	0.0008
Wnt2	1.286	0.0051

protein (MOBP), myelin oligodendrocyte glycoprotein (MOG), claudin 11 (Cldn11), and myelin regulatory factor (Myrf). The first 5 of these, which were found to be downregulated by poly(I:C) in the gene array analysis, resulted decreased by the prenatal manipulation also when analysed with real-time qRT-PCR (Fig. 3A). Ingenuity Pathway analysis (Fig. 3B) and GO enrichment analyses (Supplementary Table 2) suggested that these genes are implicated in a variety of biological processes and functions implicated in myelination and ensheathment of axons.

We further sought evidence for the possibility that changes in the expression of myelin-related genes would correlate with the behavioral and cognitive performance. In support of this notion, we found that the mRNA levels of MOG in the mPFC correlated positively with the animals' performance in the spatial recognition memory test (Supplementary Table 3). On the other hand, the gene expression levels of MOG, MAG, MAL and MOBP in the NAc showed a marked positive correlation with social approach behavior (Supplementary Table 6).

Whole-brain, voxel-wise macroscale MRI phenotyping of immune-challenged and control offspring

At 12 weeks of age, total brain volume did not significantly differ between behaviorally naïve CON ($572 \pm 7\,mm^3$) and POL offspring ($584 \pm 3\,mm^3$). Voxel-wise TBM analysis revealed sparse neuroanatomical differences in relative volume between the 2 groups ($q = 0.05$ FDR corrected; Fig. 4). Biologically plausible clusters of voxels showing apparent volume increases were present in the right hemisphere in the primary motor, somatosensory cortex (barrel field) and visual cortex (Fig. 4). In contrast, biologically plausible clusters of voxels showing apparent volume decreases were present bilaterally in the piriform cortex, anterior commissure, interfasicular nucleus, third ventricle, left periaqueductal gray nucleus, left external capsule, extending into the left fimbria, right amygdala and the right ventral mesencephalon (Fig. 4). Interestingly, the cerebellum showed the most pronounced volumetric alterations in POL offspring. Apparent volume increases were present in the crus 1 of the ansiform lobule and simple lobule and the inferior cerebellar peduncles (Fig. 4). In contrast, apparent volume decreases were present in the fifth cerebellar lobule, right paraflocculus and paramedian lobule of the cerebellum (Fig. 4).

We next tested for the presence of group-level differences between CON and POL offspring in the tissue parameters derived from the mcDESPOT dataset. Brain-wide voxel-wise
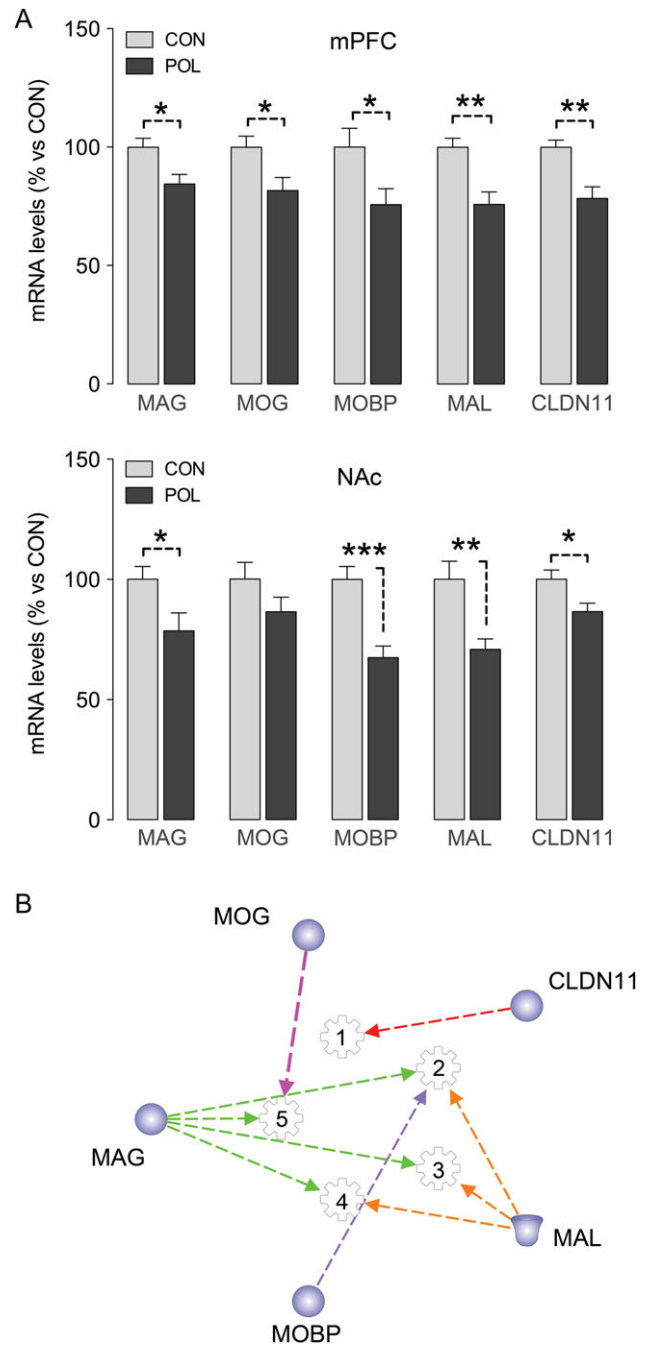

Figure 3. Validation of common myelin-related gene expression differences in the mPFC and NAc. Mice were subjected to prenatal poly(I:C) treatment on gestation day 17 (POL), or they were exposed to prenatal control (CON) treatment .(**A**) The bar plots represent the mRNA levels of each selected gene (% *versus* CON). The gene expression levels were assessed by RT-qPCR. *$P < 0.05$, **$P < 0.01$ and ***$P < 0.001$ based on independent Student's t tests (2-tailed). All data are based on N(CON) = 10, N(POL) = 10 represent means ± s.e.m. (**B**) Graphical representation of the network analysis conducted on the commonly affected myelin genes. The analysis was conducted using Ingenuity Pathway Analysis (IPA), and each gene is represented in relation to the others and to the specific functions it is involved in. **1** = Ensheathment of axons; **2** = Myelination; **3** = Myelination of cells; **4** = Myelination of nerves; **5** = Dendritic growth and branching.

cluster analysis revealed little or no change in T_1, although sparse, but biologically plausible clusters of increased T_1 (spin-lattice) relaxation time (+100 ms) were present bilaterally in the anterior nucleus accumbens and the inferior cerebellar peduncles
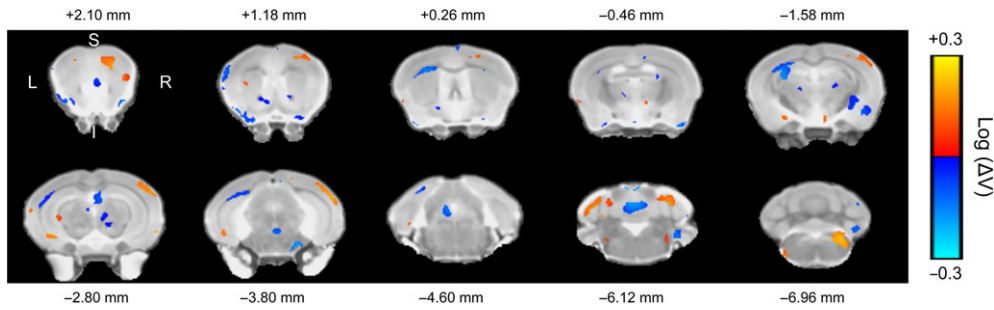
Figure 4. Sparse alterations in neuroanatomy following late prenatal immune activation revealed by brain-wide tensor based morphometry analysis of 3D FSE T_2-weighted MR images. Mice were subjected to prenatal poly(I:C) treatment on gestation day 17 (POL; N = 10), or they were exposed to prenatal control (CON, N = 10) treatment. Data shown are significant group-level voxel-wise differences in the scaled log Jacobian determinant (corrected for total brain volume) thresholded at $q < 0.05$ (FDR-corrected). Distances from bregma are indicated in mm for each slice shown. R, right; L, left; S, superior; I, inferior.
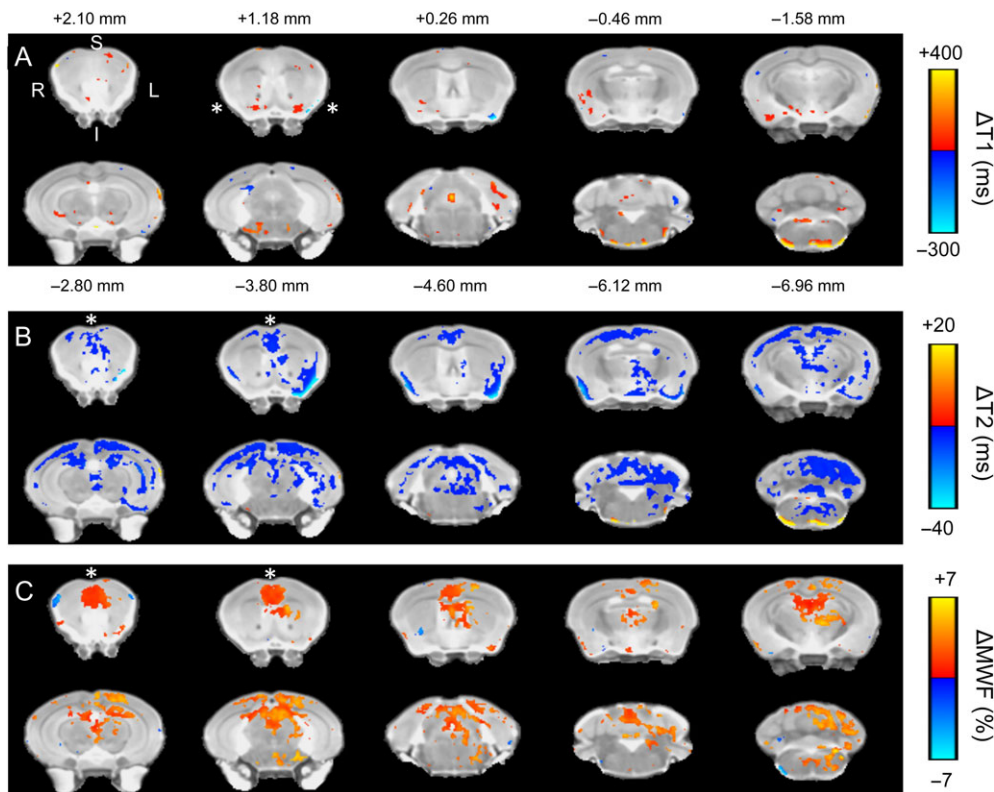
Figure 5. Alterations in (A) T_1, (B) T_2 relaxation time, and (C) myelin water fraction (MWF) following late prenatal immune activation as revealed by voxel-wise cluster analysis. Mice were subjected to prenatal poly(I:C) treatment on gestation day 17 (POL; N = 8), or they were exposed to prenatal control (CON; N = 6) treatment. Data shown are the significant voxel-wise changes in each tissue parameter relative to the control group thresholded at $q < 0.05$ (False discovery rate corrected). Distances from bregma are indicated in mm for each slice shown. R, right; L, left; S, superior; I, inferior. Changes in the medial prefrontal cortex (mPFC) and nucleus accumbens (NAc) are highlighted by the symbol (*).

($q = 0.05$ FDR corrected; Fig. 5A). In contrast, T_2 (spin–spin) relaxation times were significantly decreased in POL offspring (−20 ms) in the prefrontal, anterior cingulate, insular, retrosplenial granular, motor, somatosensory, visual and auditory cortices, with stronger decreases (−40 ms) in the piriform cortex ($q = 0.05$ FDR corrected; Fig. 5B). Bilateral decreases in T_2 (−20 ms) were also present in the hypothalamus, ventral thalamus, dorsal, and ventral hippocampus, ventral mesencephalon and cerebellar gray and white matter, respectively (Fig. 5B).

Myelin water fraction (MWF) increased significantly in POL as compared to CON offspring, particularly in the cortex, hippocampus, and cerebellar gray and white matter ($q = 0.05$ FDR corrected; Fig. 5C). These increases ranged from +2% in the prefrontal cortex to +7% in the cerebellum (Fig. 5C). Notably,

increases in MWF largely overlapped with the topographical distribution of decreases in T_2, but not T_1.

Prenatal immune activation affects protein expression levels of MOBP

Based on the preceding findings, we sought to verify whether the myelination-related changes in gene expression and MRI translate into, and stem from, differential protein expression. Thus, we analysed the protein levels of MBP, a major constituent of the myelin sheath, and MOBP, one of the candidates that emerged from our genome-wide study, with immunohistochemistry and optical densitometry (OD) in mPFC. Consistent with our gene expression study, but not the apparent increase

in MWF in the MR images, there were no significant differences in the area fraction of MBP-immunoreactive pixels in the mPFC of POL relative to CON offspring (Fig. 6**A**). In contrast, the area fraction of MOBP-immunoreactive pixels was reduced in the mPFC of POL relative to CON offspring (Fig. 6**B**).

Relationships between MRI and postmortem histology

Correlative analyses revealed a significant negative correlation between MWF (%) and T_2 (ms) in the prefrontal cortex of CON offspring, such that longer T_2 relaxation times were associated with smaller MWF (Supplementary Figure 2). These data are in good agreement with relaxometry studies in dys-myelinated mice (Shiverer mutants), which show extended T_2 relaxation times relative to their WT littermates (Dyakin et al. 2010) and our prior work in the cuprizone mouse model (Wood et al. 2016a, 2016b). T_2 relaxation time is also reported to correlate with MWF values in human datasets, although these relationships appear to be inconsistent (positive and negative) over different developmental periods (Deoni et al. 2012). A strong trend for the same relationship was also present in POL offspring (Supplementary Figure 2). There were no other significant correlations between MRI parameters (T_1, T_2, MWF, or volume) in either CON or POL offspring (*data not shown*).

We next investigated relationships between the values of T_1, T_2, and MWF against the area fraction of MBP and MOBP
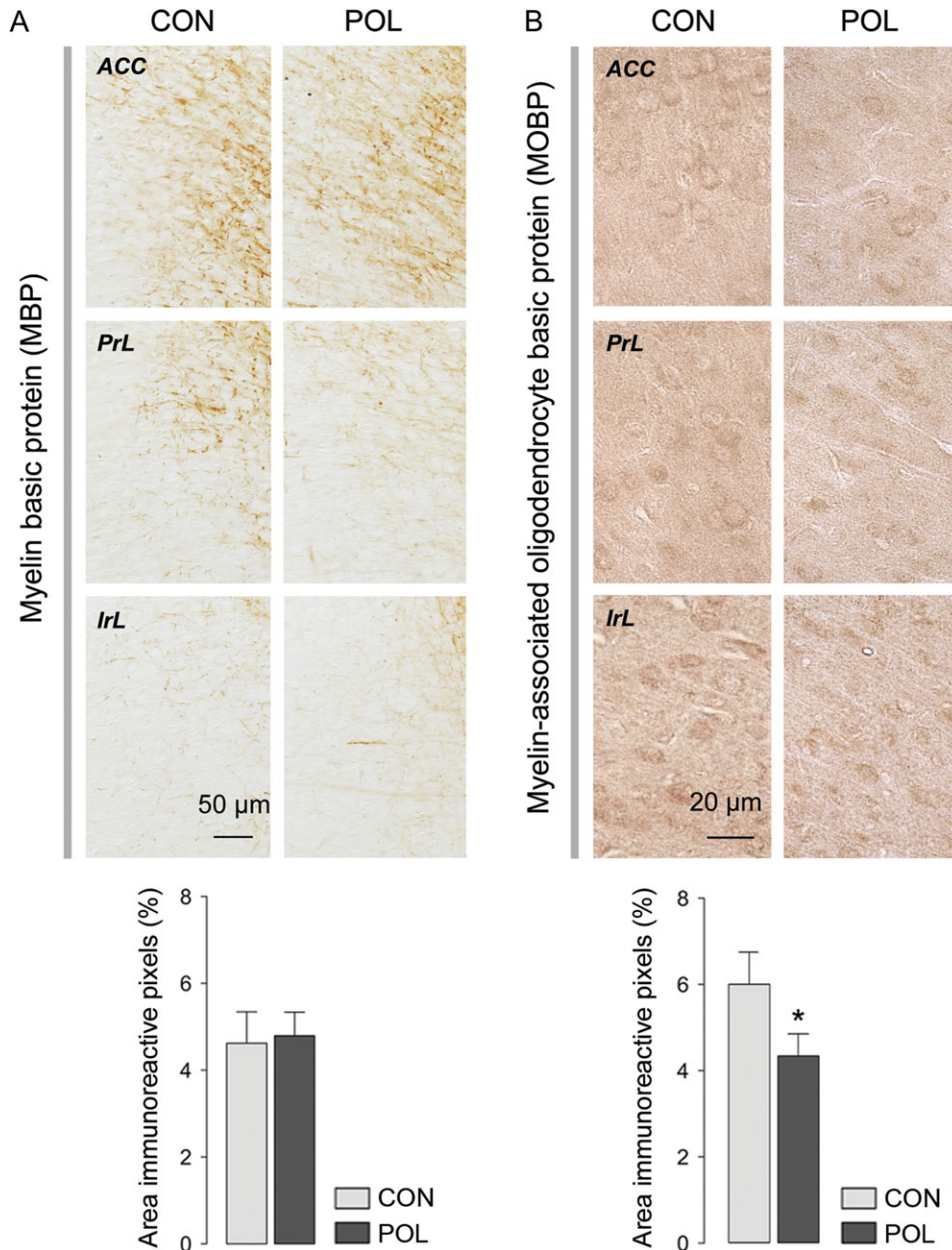

Figure 6. Immunohistochemical alterations following late prenatal immune activation. Mice were subjected to prenatal poly(I:C) treatment on gestation day 17 (POL), or they were exposed to prenatal control (CON) treatment. **(A)** The photomicrographs show representative staining of myelin basic protein (MBP) (scale bar = 50 μm), and the bar plots represent the percent area of immunoreactive pixels for MBP. N(CON) = 10, N(POL) = 9. **(B)** The photomicrographs show representative staining of myelin-associated oligodendrocyte basic protein (MOBP) (scale bar = 20 μm), and the bar plots represent the percent area of immunoreactive pixels for MOBP. *P = 0.041, N(CON) = 7 and N(POL) = 8. All data represent means ± s.e.m.

staining in the mPFC, where these data were available for the same animal. The results of this analysis are presented in Supplementary Table 9. We found no significant relationship between the measured MWF and MBP area fraction in either CON or POL offspring. In contrast, a significant negative correlation was found between T_2 and MOBP area fraction in the mPFC of POL offspring, such that shorter T_2 values were associated with a greater area fraction of MOBP (Supplementary table 9). The T_1 values in the mPFC were also negatively related to MOBP area fraction in POL offspring, although this failed to reach statistical significance at the 2-tailed level ($r = -0.739$; $P = 0.09$; Supplementary Table 9)

Prenatal immune activation alters the methylation profile of the MOBP promoter

We were further interested in examining whether epigenetic modifications may be a plausible mechanism underlying the transcriptional effects of prenatal immune activation. To test this hypothesis, we analysed DNA methylation profiles of the MOBP promoter in the mPFC and NAc using the EpiTYPER technique, which detects and quantifies DNA methylation using MALDI-TOF mass spectrometry (Suchiman et al. 2015). We focused on MOBP because the initial microarray and subsequent RT-PCR analyses consistently revealed decreased expression of this myelination-related gene in offspring exposed to prenatal immune activation relative to control offspring (Figs 2A and 3A).

We found hypermethylation of multiple CpGs sites in 2 distinct MOBP promoter segments that are adjacent to (amplicon 1) or incorporate (amplicon 2) the transcriptional start site (TSS) (Fig. 7). In the mPFC, the infection-induced changes in CpG methylation levels differed as a function of genomic location: The percent CpG methylation encompassed in amplicon 1 was increased at CpG_{507} and CpG_{457} in POL compared to CON offspring, whereas it was decreased at CpG_{343} in the former relative to the latter group (Fig. 7**B**). On the other hand, the CpG sites encompassed in amplicon 2 were generally hypermethylated in POL relative to CON offspring (Fig. 7**B**). Prenatal immune activation also led to genomic location-dependent changes in accumbal MOBP DNA methylation: the methylation levels at CpG_{239} (amplicon 1) and at CpG_{210} (amplicon 2) were increased in POL compared to CON offspring (Fig. 7**C**).

We further investigated whether the infection-induced changes in DNA methylation might correlate with the gene expression levels of MOBP and with the animals' behavioral performance. As summarized in Supplementary Table 4 and Supplementary Table 5, the methylation levels of CpG_{457} positively correlated with the expression levels of MOBP in the mPFC, whereas the methylation levels of CpG_{343} negatively correlated with the animals' performance in the spatial recognition memory test. There were no significant correlations between MOBP DNA methylation and gene expression levels in the NAc, nor were there any significant correlations between accumbal DNA methylation and behavioral performances of primary interest (Supplementary Table 7 and 8).
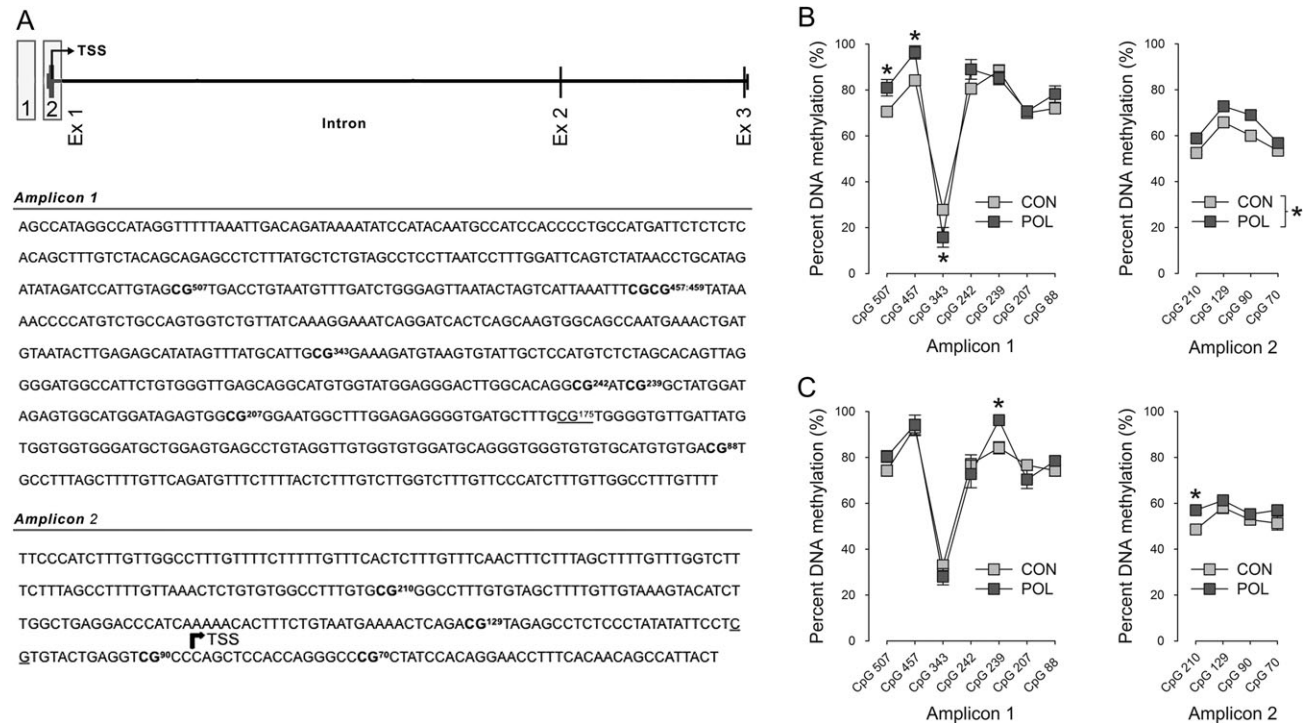

Figure 7. Investigation of DNA methylation differences in the promoter of the MOBP gene using EpiTYPER. Mice were subjected to prenatal poly(I:C) treatment on gestation day 17 (POL), or they were exposed to prenatal control (CON) treatment. (**A**) Graphical representation of the MOBP gene and genomic locations of the selected amplicons. Sequences of the selected amplicons and position of investigated CpGs in each amplicon. Methylation of the numbered CpGs (in bold font) was accessible to quantification by EpiTYPER, whereas underlined CpGs were un-measurable for technical reasons. (**B**) Percent DNA methylation of specific CpGs in the medial prefrontal cortex. Amplicon 1: *$P < 0.05$, based on post hoc comparisons at each individual CpG site following the presence of a significant interaction between prenatal treatment and CpG region ($F_{(6,54)} = 5.35$, $P < 0.001$); amplicon 2: *$P < 0.05$, reflecting the significant main effects of prenatal treatment ($F_{(1,9)} = 7.32$, $P < 0.05$). (**C**) Percent DNA methylation of specific CpGs in the nucleus accumbens. *$P < 0.05$, based on post hoc comparisons at each individual CpG site following the presence of a significant interaction between prenatal treatment and CpG region (amplicon 1: $F_{(6,54)} = 2.52$, $P < 0.05$; amplicon 2: $F_{(3,27)} = 2.45$, $P < 0.05$). All data are based on $N(CON) = 6$ and $N(POL) = 5$ and reflect means ± s.e.m.

Discussion

The present study analysed the gene expression profiles of the mPFC and NAc following exposure to late prenatal immune activation, and implemented a multi-system approach based on MR imaging, immunohistochemistry and epigenetic analyses to follow-up the gene expression changes it uncovered. Late prenatal immune activation led to a dysregulation of a variety of different genes in both brain areas, and to common prefrontal and striatal changes in myelin markers of functionality and stability. These findings were confirmed and extended by MRI and immunohistochemical results, while epigenetic analyses pointed to altered DNA methylation as a putative molecular mechanism underlying some of the transcriptional effects. Our study thus adds to the characterization of the long-lasting molecular signatures of late prenatal immune activation in adult corticostriatal regions.

Our transcriptomic and epigenetic analyses in immune-challenged and control offspring were conducted using behaviorally and cognitively characterized animals. Advantages of this approach include that the examination of possible molecular effects takes place against the background of overt behavioral and cognitive phenotypes, which appears particularly important for (immune-mediated) neurodevelopmental disruption models that may contain a certain degree of litter-to-litter variability (Meyer et al. 2009). Here, we confirmed the deleterious effects of prenatal poly(I:C) exposure on spatial short-term memory and social interaction (Bitanihirwe et al. 2010a, 2010b; Richetto et al. 2013), suggesting that prenatal viral-like immune activation leads to robust deficits in these cognitive and behavioral domains. Against the background of these impairments, we further identified transcriptomic, epigenetic, and neuroanatomical abnormalities in offspring exposed to prenatal immune activation. This approach thus allowed us to assess possible molecular correlates of the behavioral and cognitive abnormalities induced by prenatal immune challenge. For example, we identified a positive correlation between accumbal (and, to a lesser extent, prefrontal) expression levels of myelination-related genes such as MAG, MOG, MOBP and MAL and the animals' behavioral performance, especially when considering the domains of social interaction. These correlations, however, should be interpreted with caution in view of the relatively modest group sizes.

Our genome-wide gene expression analyses revealed transcriptomic alterations in a number of genes, many of which have been associated with schizophrenia. In particular, when comparing our results with the currently recognized risk genes for schizophrenia, 5 of the affected genes in the mPFC (ADORA2A, CNP, DRD2, MAG, PPP1RB1), and 21 of the affected genes in the NAc (APOD, CACNA 1B, DRD3, FOXP2, GLS, GRIN2A, HIST1H2BC, HRT1A, HRT2A, HRT4, MAG, MGST1, MYO16, OXT, PBRM1, PDYN, ST3GAL1, SULT4A1, TSNAX, VAMP4) fall into this list (Butler et al. 2016). In agreement with previous reports by Connor et al. (2012) and Smith et al. (2007), prenatal immune activation leads to less extensive gene expression changes in the mPFC ($n = 116$ genes) as compared to the NAc ($n = 251$ genes) (Smith et al. 2007; Connor et al. 2012). Moreover, consistent with these earlier reports (Connor et al. 2012), most transcripts in prenatally infected offspring show less than 2-fold changes from the control group. Such effect sizes are not unprecedented given the early prenatal timing of the environmental insult, which typically leads to pathological changes in brain and behavior that are widespread but often relatively mild in terms of effect size (Meyer et al. 2007).

Despite the magnitude and number of changes, these effects may still be pathophysiologically relevant and may prime the organism to altered neuronal functions when challenged with other environmental stressors or behavioral and cognitive demands.

Notably, some of our data are consistent with previous findings in the prenatal influenza infection model developed by Fatemi and colleagues, suggesting that at least parts of the transcriptomic changes induced by prenatal influenza exposure may be mediated indirectly via activation of the maternal immune system (Fatemi et al. 2012). As in the prenatal influenza model, we observed changes in the expression of FOXP2, PPP1R1B, DEAD box polypeptide, ATP13, CRYGE, and various other genes implicated in the pathophysiology of schizophrenia and autism (Fatemi et al. 2005, 2008, 2009a, 2009b). The similarities between the 2 models are even more evident when considering the region-overlapping transcriptomic effects identified here. Indeed, among the 14 genes commonly affected in the mPFC and NAc, 6 of these (MAG, MOG, MOBP, MAL, CLDN11 and MYRF) are similarly affected by prenatal exposure to influenza (Fatemi et al. 2005, 2009a) and are involved in myelin functionality and stability. The consistency between our findings and those reported by Fatemi and colleagues thus suggests that reduced expression of markers of myelin stability and functionality could be a long-lasting molecular signature of various prenatal immune challenges. Additional support for this hypothesis also stems from recent proteomic analyses demonstrating similar effects of prenatal viral-like immune activation on myelination-related proteins (Farrelly et al. 2015). Indeed, Farrelly et al. (2015) also uncovered changes in myelin-related proteins, such as MBP1 and rhombex 29, suggesting that prenatal infection may contribute to neurodevelopmental abnormalities through mechanisms involving myelin formation and functionality (Farrelly et al. 2015).

The effects of prenatal immune activation on myelin-related dysfunctions are particularly interesting in light of the potential role of myelination and white matter abnormalities present in schizophrenia and other neurodevelopmental disorders (Haroutunian et al. 2014; Mighdoll et al. 2015; Chavarria-Siles et al. 2016). Indeed, myelin provides the basis for rapid impulse conduction in the central nervous system and acts as electrical insulation for the unsheathed axon, which both helps to preserve the amplitude and increase the conduction velocity of the propagating axonal potential (Nave and Werner 2014; Normand and Rasband 2015). Given these essential functions, it is not surprising that damage to the myelin structure has been implicated in a variety of neurodevelopmental disorders. The expression of MAG, MOG, MOBP, MAL and CLDN11 is physiologically enriched in myelin-forming oligodendrocytes and is downregulated in schizophrenic subjects (Hakak et al. 2001; Aston et al. 2004; Katsel et al. 2005; Le-Niculescu et al. 2009). Moreover, alterations in white matter, such as volume reductions in prefrontal areas and increased density in subcortical areas, morphologic abnormalities in oligodendroglia and myelin-related gene abnormalities have all been related to schizophrenia (Sanfilipo 2000a, 2000b; Davis and Haroutunian 2003; Davis et al. 2003; Connor et al. 2011). Our findings here, together with those reported by Fatemi et al. and Farrelly et al. (Fatemi et al. 2005, 2009a, 2009b; Farrelly et al. 2015), highlight that the pathological relationship between prenatal infection and neurodevelopmental psychiatric disorders involves the disruption of myelination-related processes.

We performed additional MRI and immunohistochemical investigations to examine whether abnormal expression of

myelination-related genes may have an impact on gray and white matter structure. In general, our brain-wide voxel-wise analysis revealed sparse differences in volume and T_1, but widespread decreases in T_2 and increases in the MWF between CON and POL offspring. In the NAc, we observed focal increases in T_1, decreases in T_2, but no change in the MWF, whereas the mPFC of POL offspring showed significant decreases in T_2 and an apparent increase in the MWF. Our data represent the first application of mcDEPOST to a rodent model of an epidemiologically informed risk factor for neurodevelopmental disorders. A single prior clinical study has utilized mcDESPOT in a small number of adult individuals with ASD ($N = 14$) (Deoni et al. 2015). This revealed increases in T_1 bilaterally within the cerebellum, thalamus, and internal capsule; and in right temporal and occipital WM, accompanied by decreases in the MWF, but no change in T_2. Our T_1 data, especially in the cerebellum, thus partially overlap with these data, but the majority of our findings go in the opposite direction. This may not be surprising since we only model a single disease factor, whereas most neurodevelopmental disorders such as ASD are clearly multifactorial in origin.

A previous longitudinal *in vivo* MRI study in rats has demonstrated that exposure to poly(I:C)-induced immune activation on GD 15 leads to an abnormal developmental trajectory of brain maturation (Piontkewitz et al. 2011). This raises the question of whether our cross-sectional MRI data are representative of a similar phenomenon in the mouse brain following immune activation on GD 17. Longitudinal *in vivo* MRI studies of typically maturing C57/Bl6 mice suggest 2 important findings in this context. First, most gray matter regions reach their final volume within the first 8 postnatal weeks (Hammelrath et al. 2015). Second, there is an initial decrease in T_2 from 3 to 8 weeks postnatal, after which T_2 steadily increases up to 24 weeks of age (Hammelrath et al. 2015). Taken together, our findings of widespread decreases in T_2 in POL offspring at 12 weeks postnatal suggest a delay in the normal process of mouse brain maturation following maternal immune activation. Although longitudinal *in vivo* MRI studies will be helpful to clarify this, we have recently shown that prenatal immune activation on GD 17 in mice leads to an "immature" cortical GABAergic network in early adulthood, supporting a "delayed maturation" hypothesis (Richetto et al., 2014). Importantly, rats and mice show differential timescales of brain maturation, thus these findings may not translate precisely across species (Mengler et al. 2014; Hammelrath et al. 2015)

How do these macroscale findings relate to those at the transcriptional level, particularly with respect to myelination? Our postmortem immunohistochemistry analysis of the mPFC is in line with the gene expression data, with no change in MBP, but a decrease in MOBP. What then, underlines the changes in T_1 and T_2, and in particular the seemingly paradoxical increase in the MWF in the PFC of POL offspring? Prior studies have shown that the MWF derived from a conventional multiple spin-echo MCR approach are strongly correlated with histological estimates of myelin content (Webb et al. 2003; Stanisz et al. 2004; Laule et al. 2008, 2006), but to the best of our knowledge this has not been done for the mcDESPOT MCR technique. We have recently shown that the mcDESPOT-derived MWF is sensitive to demyelination of white matter tracts in the mouse brain induced by chronic cuprizone exposure (Wood et al. 2016a, 2016b). Specifically, demyelinated regions showed higher values of T_1 and T_2, with a corresponding decrease in the MWF (Wood et al. 2016a, 2016b). In the current study, we observed increases in T_1 and decreases in T_2 in

the NAc and mPFC, respectively (as well as in other brain regions). Although preliminary, due to low statistical power, our correlation analysis suggests that the increase in prefrontal MWF signals is not related to the area fraction of MBP, but is negatively correlated to T_2 in both CON and POL offspring. Furthermore, there is a negative correlation between MOBP area fraction and T_2 in the PFC in POL offspring only. These data are in good agreement with observations that T_1 and T_2 are influenced by the entry of precursory macromolecules for myelin and myelin-associated proteins during human brain maturation (Paus et al. 2001). Furthermore, this is consistent with the robust topographical overlap between decreases in T_2 and apparent increases in the MWF in our MRI dataset.

Taken together, this suggests that the increase in MWF is not caused by an increase in the quantity of myelin itself, but changes to its 'quality'. Speculatively, decreased levels of myelin stability proteins would be predicted to affect the microstructure of the myelin sheath, altering the g-ratio. For example, if the myelin sheath is less compact, the fraction of water trapped between lipid bilayers could potentially increase, thereby driving an apparent MWF increase. Importantly, The function of MOBP has been associated with the compaction and stabilization of myelin membranes (Gould et al. 2000; Montague et al. 2006). This hypothesis could be tested by exploiting recent advances in the combination of myelin content information (obtained with mcDESPOT MCR) with information about axonal microstructure obtained through multi-shell DTI (Melbourne et al. 2014; Dean et al. 2016). Changes in the relaxation properties of brain tissues may however also reflect other biological processes, including iron accumulation and changes in tissue water compartmentalization through changes in axon fiber size, density or coherence (Paus et al. 2001; MacKay et al. 2006). Whilst further investigations are therefore warranted, our current data provide initial evidence suggesting that abnormal expression of myelination-related genes can be plausibly linked to changes in tissue relaxation time. Nevertheless, they also show that further validation of the mcDESPOT model at the postmortem level in rodent models would be helpful to the field.

Lastly, our study provides the first report concerning hypermethylation of the MOBP promoter following prenatal immune activation. Hence, we identify an epigenetic mechanism that could possibly underlie the effects of prenatal infection on long-lasting transcriptomic changes in myelination-related genes. The identified correlations between MOBP DNA methylation and mRNA levels readily support this notion. It should be pointed out, however, that the correlative analyses between DNA methylation and gene expression levels were based on small sample sizes ($N = 5–6$ animals per group), and therefore, they might have been underpowered. Nevertheless, our findings are in agreement with previous studies showing prenatal immune activation in rats or mice can induce that various epigenetic changes such as DNA hyper- or hypomethylation, histone modifications, and altered micro-RNA expression, some of which likely affect the expression of corresponding genes (Connor et al. 2012; Tang et al. 2013; Basil et al. 2014; Labouesse et al. 2015; Richetto et al., 2016).

In conclusion, our study further characterizes the molecular signature of prenatal viral-like immune activation in the offspring's corticostriatal regions. In particular, prenatal infection-induced transcriptomic changes in myelination-related genes seems to be a common pathological feature in multiple brain areas. The current study also provides the first voxel-wise assessment of brain volume and application of MCR methodology,

which together suggest a putative delay in brain maturation following prenatal viral-like infection. Furthermore, the study provides preliminary evidence that these macrostructural abnormalities may be plausibly linked to abnormal expression of myelination-related genes in the absence of demyelination *per se*. Future investigations are therefore needed to confirm the mechanistic links between these molecular modifications and MR-detectable brain alterations occurring in prenatally infected offspring. Nevertheless, our data highlight the power of combining system level assessments (MRI) with invasive cellular and molecular phenotyping of the same animal *postmortem* in the elucidation of disease-relevant mechanisms.

Supplementary Material

Supplementary material can be found at: http://www.cercor. oxfordjournals.org/.

References

Aston C, Jiang L, Sokolov BP. 2004. Microarray analysis of post-mortem temporal cortex from patients with schizophrenia. J Neurosci Res. 77:858–866.

Ballesteros MC, Hansen PE, Soila K. 1993. MR imaging of the developing human brain. Part 2. Postnatal development. Radiographics. 13:611–622.

Basil P, Li Q, Dempster EL, Mill J, Sham PC, Wong CC, McAlonan GM. 2014. Prenatal maternal immune activation causes epigenetic differences in adolescent mouse brain. Transl Psychiatry. 4:e434.

Bitanihirwe BK, Peleg-Raibstein D, Mouttet F, Feldon J, Meyer U. 2010a. Late prenatal immune activation in mice leads to behavioral and neurochemical abnormalities relevant to the negative symptoms of schizophrenia. Neuropsychopharmacology. 35:2462–2478.

Bitanihirwe BK, Weber L, Feldon J, Meyer U. 2010b. Cognitive impairment following prenatal immune challenge in mice correlates with prefrontal cortical AKT1 deficiency. Int J Neuropsychopharmacol. 13:981–996.

Brown AS. 2011. The environment and susceptibility to schizophrenia. Prog Neurobiol. 93:23–58.

Brown AS, Derkits EJ. 2010. Prenatal infection and schizophrenia: a review of epidemiologic and translational studies. Am J Psychiatry. 167:261–280.

Butler MG, McGuire AB, Masoud H, Manzardo AM. 2016. Currently recognized genes for schizophrenia: High-resolution chromosome ideogram representation. Am J Med Genet B Neuropsychiatr Genet. 171B:181–202.

Chavarria-Siles I, White T, de Leeuw C, Goudriaan A, Lips E, Ehrlich S, Turner JA, Calhoun VD, Gollub RL, Magnotta VA, et al. 2016. Myelination-related genes are associated with decreased white matter integrity in schizophrenia. Eur J Hum Genet. 24:381–386.

Connor CM, Crawford BC, Akbarian S. 2011. White matter neuron alterations in schizophrenia and related disorders. Int J Dev Neurosci. 29:325–334.

Connor CM, Dincer A, Straubhaar J, Galler JR, Houston IB, Akbarian S. 2012. Maternal immune activation alters behavior in adult offspring, with subtle changes in the cortical transcriptome and epigenome. Schizophr Res. 140:175–184.

Davis KL, Haroutunian V. 2003. Global expression-profiling studies and oligodendrocyte dysfunction in schizophrenia and bipolar disorder. Lancet. 362:758.

Davis KL, Stewart DG, Friedman JI, Buchsbaum M, Harvey PD, Hof PR, Buxbaum J, Haroutunian V. 2003. White matter changes in schizophrenia: evidence for myelin-related dysfunction. Arch Gen Psychiatry. 60:443–456.

Dean DC 3rd, O'Muircheartaigh J, Dirks H, Travers BG, Adluru N, Alexander AL, Deoni SC. 2016. Mapping an index of the myelin g-ratio in infants using magnetic resonance imaging. NeuroImage. 132:225–237.

Deoni SC, Dean DC 3rd, O'Muircheartaigh J, Dirks H, Jerskey BA. 2012. Investigating white matter development in infancy and early childhood using myelin water faction and relaxation time mapping. Neuroimage. 63:1038–1053.

Deoni SC, Matthews L, Kolind SH. 2013. One component? Two components? Three? The effect of including a nonexchanging "free" water component in multicomponent driven equilibrium single pulse observation of T1 and T2. Magn Reson Med. 70:147–154.

Deoni SC, Mercure E, Blasi A, Gasston D, Thomson A, Johnson M, Williams SC, Murphy DG. 2011. Mapping infant brain myelination with magnetic resonance imaging. J Neurosci. 31:784–791.

Deoni SC, Rutt BK, Arun T, Pierpaoli C, Jones DK. 2008a. Gleaning multicomponent T1 and T2 information from steady-state imaging data. Magn Reson Med. 60:1372–1387.

Deoni SC, Williams SC, Jezzard P, Suckling J, Murphy DG, Jones DK. 2008b. Standardized structural magnetic resonance imaging in multicentre studies using quantitative T1 and T2 imaging at 1.5 T. Neuroimage. 40:662–671.

Deoni SC, Zinkstok JR, Daly E, Ecker C, Consortium MA, Williams SC, Murphy DG. 2015. White-matter relaxation time and myelin water fraction differences in young adults with autism. Psychol Med. 45:795–805.

Dyakin VV, Chen Y, Branch CA, Veeranna, Yuan A, Rao M, Kumar A, Peterhoff CM, Nixon RA. 2010. The contributions of myelin and axonal caliber to transverse relaxation time in shiverer and neurofilament-deficient mouse models. NeuroImage. 51:1098–1105.

Eyles D, Feldon J, Meyer U. 2012. Schizophrenia: do all roads lead to dopamine or is this where they start? Evidence from two epidemiologically informed developmental rodent models. Transl Psychiatry. 2:e81.

Farrelly L, Focking M, Piontkewitz Y, Dicker P, English J, Wynne K, Cannon M, Cagney G, Cotter DR. 2015. Maternal immune activation induces changes in myelin and metabolic proteins, some of which can be prevented with risperidone in adolescence. Dev Neurosci. 37:43–55.

Fatemi SH, Folsom TD, Reutiman TJ, Abu-Odeh D, Mori S, Huang H, Oishi K. 2009a. Abnormal expression of myelination genes and alterations in white matter fractional anisotropy following prenatal viral influenza infection at E16 in mice. Schizophr Res. 112:46–53.

Fatemi SH, Folsom TD, Reutiman TJ, Huang H, Oishi K, Mori S. 2009b. Prenatal viral infection of mice at E16 causes changes in gene expression in hippocampi of the offspring. Eur Neuropsychopharmacol. 19:648–653.

Fatemi SH, Folsom TD, Rooney RJ, Mori S, Kornfield TE, Reutiman TJ, Kneeland RE, Liesch SB, Hua K, Hsu J, et al. 2012. The viral theory of schizophrenia revisited: abnormal placental gene expression and structural changes with lack of evidence for H1N1 viral presence in placentae of infected mice or brains of exposed offspring. Neuropharmacology. 62:1290–1298.

Fatemi SH, Pearce DA, Brooks AI, Sidwell RW. 2005. Prenatal viral infection in mouse causes differential expression of genes

in brains of mouse progeny: a potential animal model for schizophrenia and autism. Synapse. 57:91–99.

Fatemi SH, Reutiman TJ, Folsom TD, Huang H, Oishi K, Mori S, Smee DF, Pearce DA, Winter C, Sohr R, et al. 2008. Maternal infection leads to abnormal gene regulation and brain atrophy in mouse offspring: implications for genesis of neurodevelopmental disorders. Schizophr Res. 99:56–70.

Genovese CR, Lazar NA, Nichols T. 2002. Thresholding of statistical maps in functional neuroimaging using the false discovery rate. Neuroimage. 15:870–878.

Giovanoli S, Engler H, Engler A, Richetto J, Voget M, Willi R, Winter C, Riva MA, Mortensen PB, Feldon J, et al. 2013. Stress in puberty unmasks latent neuropathological consequences of prenatal immune activation in mice. Science. 339:1095–1099.

Gould RM, Freund CM, Palmer F, Feinstein DL. 2000. Messenger RNAs located in myelin sheath assembly sites. J Neurochem. 75:1834–1844.

Hakak Y, Walker JR, Li C, Wong WH, Davis KL, Buxbaum JD, Haroutunian V, Fienberg AA. 2001. Genome-wide expression analysis reveals dysregulation of myelination-related genes in chronic schizophrenia. Proc Natl Acad Sci U S A. 98:4746–4751.

Hammelrath L, Skokic S, Khmelinskii A, Hess A, van der Knaap N, Staring M, Lelieveldt BP, Wiedermann D, Hoehn M. 2015. Morphological maturation of the mouse brain: An in vivo MRI and histology investigation. NeuroImage. 125:144–152.

Haroutunian V, Katsel P, Roussos P, Davis KL, Altshuler LL, Bartzokis G. 2014. Myelination, oligodendrocytes, and serious mental illness. Glia. 62:1856–1877.

Harvey L, Boksa P. 2012. A stereological comparison of GAD67 and reelin expression in the hippocampal stratum oriens of offspring from two mouse models of maternal inflammation during pregnancy. Neuropharmacology. 62:1767–1776.

Horvath S, Mirnics K. 2015. Schizophrenia as a disorder of molecular pathways. Biol Psychiatry. 77:22–28.

Ibi D, Yamada K. 2015. Therapeutic Targets for Neurodevelopmental Disorders Emerging from Animal Models with Perinatal Immune Activation. Int J Mol Sci. 16: 28218–28229.

Katsel P, Davis KL, Haroutunian V. 2005. Variations in myelin and oligodendrocyte-related gene expression across multiple brain regions in schizophrenia: a gene ontology study. Schizophr Res. 79:157–173.

Labouesse MA, Dong E, Grayson DR, Guidotti A, Meyer U. 2015. Maternal immune activation induces GAD1 and GAD2 promoter remodeling in the offspring prefrontal cortex. Epigenetics. 10:1143–1155.

Laule C, Kozlowski P, Leung E, Li DK, Mackay AL, Moore GR. 2008. Myelin water imaging of multiple sclerosis at 7 T: correlations with histopathology. Neuroimage. 40:1575–1580.

Laule C, Leung E, Lis DK, Traboulsee AL, Paty DW, MacKay AL, Moore GR. 2006. Myelin water imaging in multiple sclerosis: quantitative correlations with histopathology. Mult Scler. 12:747–753.

Le-Niculescu H, Patel SD, Bhat M, Kuczenski R, Faraone SV, Tsuang MT, McMahon FJ, Schork NJ, Nurnberger JI Jr, Niculescu AB 3rd. 2009. Convergent functional genomics of genome-wide association data for bipolar disorder: comprehensive identification of candidate genes, pathways and mechanisms. Am J Med Genet B Neuropsychiatr Genet. 150B:155–181.

Leppert IR, Almli CR, McKinstry RC, Mulkern RV, Pierpaoli C, Rivkin MJ, Pike GB. 2009. T(2) relaxometry of normal pediatric brain development. J Magn Reson Imaging. 29:258–267.

MacKay A, Laule C, Vavasour I, Bjarnason T, Kolind S, Madler B. 2006. Insights into brain microstructure from the T2 distribution. Magn Reson Imaging. 24:515–525.

Marangoni C, Hernandez M, Faedda GL. 2016. The role of environmental exposures as risk factors for bipolar disorder: A systematic review of longitudinal studies. J Affect Disord. 193:165–174.

Melbourne A, Eaton-Rosen Z, De Vita E, Bainbridge A, Cardoso MJ, Price D, Cady E, Kendall GS, Robertson NJ, Marlow N, et al. 2014. Multi-modal measurement of the myelin-to-axon diameter g-ratio in preterm-born neonates and adult controls. Med Image Comput Compu Assist Interv. 17: 268–275.

Mengler L, Khmelinskii A, Diedenhofen M, Po C, Staring M, Lelieveldt BP, Hoehn M. 2014. Brain maturation of the adolescent rat cortex and striatum: changes in volume and myelination. Neuroimage. 84:35–44.

Meyer U. 2014. Prenatal poly(i:C) exposure and other developmental immune activation models in rodent systems. Biol Psychiatry. 75:307–315.

Meyer U, Feldon J, Fatemi SH. 2009. In-vivo rodent models for the experimental investigation of prenatal immune activation effects in neurodevelopmental brain disorders. Neurosci Biobehav Rev. 33:1061–1079.

Meyer U, Feldon J. 2010. Epidemiology-driven neurodevelopmental animal models of schizophrenia. Prog Neurobiol. 90: 285–326.

Meyer U, Feldon J, Schedlowski M, Yee BK. 2005. Towards an immuno-precipitated neurodevelopmental animal model of schizophrenia. Neurosci Biobehav Rev. 29:913–947.

Meyer U, Nyffeler M, Engler A, Urwyler A, Schedlowski M, Knuesel I, Yee BK, Feldon J. 2006. The time of prenatal immune challenge determines the specificity of inflammation-mediated brain and behavioral pathology. J Neurosci. 26:4752–4762.

Meyer U, Nyffeler M, Yee BK, Knuesel I, Feldon J. 2008. Adult brain and behavioral pathological markers of prenatal immune challenge during early/middle and late fetal development in mice. Brain Behav Immun. 22:469–486.

Meyer U, Yee BK, Feldon J. 2007. The neurodevelopmental impact of prenatal infections at different times of pregnancy: the earlier the worse? Neuroscientist. 13:241–256.

Mighdoll MI, Tao R, Kleinman JE, Hyde TM. 2015. Myelin, myelin-related disorders, and psychosis. Schizophr Res. 161: 85–93.

Montague P, McCallion AS, Davies RW, Griffiths IR. 2006. Myelin-associated oligodendrocytic basic protein: a family of abundant CNS myelin proteins in search of a function. Dev Neurosci. 28:479–487.

Nave KA, Werner HB. 2014. Myelination of the nervous system: mechanisms and functions. Annu Rev Cell Dev Biol. 30: 503–533.

Normand EA, Rasband MN. 2015. Subcellular patterning: axonal domains with specialized structure and function. Dev Cell. 32:459–468.

Patterson PH. 2011. Maternal infection and immune involvement in autism. Trends Mol Med. 17:389–394.

Paus T, Collins DL, Evans AC, Leonard G, Pike B, Zijdenbos A. 2001. Maturation of white matter in the human brain: a review of magnetic resonance studies. Brain Res Bull. 54: 255–266.

Peleg-Raibstein D, Feldon J, Meyer U. 2012. Behavioral animal models of antipsychotic drug actions. Handb Exp Pharmacol. 212:361–406.

Piontkewitz Y, Arad M, Weiner I. 2011. Abnormal trajectories of neurodevelopment and behavior following in utero insult in the rat. Biol Psychiatry. 70:842–851.

Richetto J, Calabrese F, Meyer U, Riva MA. 2013. Prenatal versus postnatal maternal factors in the development of infection-induced working memory impairments in mice. Brain Behav Immun. 33:190–200.

Richetto J, Calabrese F, Riva MA, Meyer U. 2014. Prenatal immune activation induces maturation-dependent alterations in the prefrontal GABAergic transcriptome. Schizophr Bull. 40:351–361.

Richetto J, Labouesse MA, Poe MM, Cook JM, Grace AA, Riva MA, Meyer U. 2015. Behavioral effects of the benzodiazepine-positive allosteric modulator SH-053-2′F-S-CH(3) in an immune-mediated neurodevelopmental disruption model. Int J Neuropsychopharmacol. 18. pii: pyu055.

Richetto J, Massart R, Weber-Stadlbauer U, Szyf M, Riva MA, Meyer U. 2016. Genome-Wide DNA Methylation Changes in a Mouse Model of Infection-Mediated Neurodevelopmental Disorders. Biol Psychiatry, (in press).

Richey JA, Damiano CR, Sabatino A, Rittenberg A, Petty C, Bizzell J, Voyvodic J, Heller AS, Coffman MC, Smoski M, et al. 2015. Neural Mechanisms of Emotion Regulation in Autism Spectrum Disorder. J Autism Dev Disord. 45:3409–3423.

Sanfilipo M, Lafargue T, Arena L, Rusinek H, Kushner K, Lautin A, Loneragan C, Vaid G, Rotrosen J, Wolkin A. 2000a. Fine volumetric analysis of the cerebral ventricular system in schizophrenia: further evidence for multifocal mild to moderate enlargement. Schizophr Bull. 26:201–216.

Sanfilipo M, Lafargue T, Rusinek H, Arena L, Loneragan C, Lautin A, Feiner D, Rotrosen J, Wolkin A. 2000b. Volumetric measure of the frontal and temporal lobe regions in schizophrenia: relationship to negative symptoms. Arch Gen Psychiatry. 57:471–480.

Schubert D, Martens GJ, Kolk SM. 2015. Molecular underpinnings of prefrontal cortex development in rodents provide insights into the etiology of neurodevelopmental disorders. Mol Psychiatry. 20:795–809.

Selemon LD, Zecevic N. 2015. Schizophrenia: a tale of two critical periods for prefrontal cortical development. Transl Psychiatry. 5:e623.

Smith SE, Li J, Garbett K, Mirnics K, Patterson PH. 2007. Maternal immune activation alters fetal brain development through interleukin-6. J Neurosci. 27:10695–10702.

Smith SM, Nichols TE. 2009. Threshold-free cluster enhancement: addressing problems of smoothing, threshold dependence and localisation in cluster inference. NeuroImage. 44:83–98.

Stanisz GJ, Webb S, Munro CA, Pun T, Midha R. 2004. MR properties of excised neural tissue following experimentally induced inflammation. Magn Reson Med. 51:473–479.

Suchiman HE, Slieker RC, Kremer D, Slagboom PE, Heijmans BT, Tobi EW. 2015. Design, measurement and processing of region-specific DNA methylation assays: the mass spectrometry-based method EpiTYPER. Front Genet. 6:287.

Tang B, Jia H, Kast RJ, Thomas EA. 2013. Epigenetic changes at gene promoters in response to immune activation in utero. Brain Behav Immun. 30:168–175.

Tebbenkamp AT, Willsey AJ, State MW, Sestan N. 2014. The developmental transcriptome of the human brain: implications for neurodevelopmental disorders. Curr Opin Neurol. 27:149–156.

Turkheimer FE, Leech R, Expert P, Lord LD, Vernon AC. 2015. The brain's code and its canonical computational motifs. From sensory cortex to the default mode network: A multi-scale model of brain function in health and disease. Neurosci Biobehav Rev. 55:211–222.

Webb S, Munro CA, Midha R, Stanisz GJ. 2003. Is multicomponent T2 a good measure of myelin content in peripheral nerve? Magn Reson Med. 49:638–645.

Wood TC, Simmons C, Torres J, FDA, Vernon AC, Hurley SA, Williams SC, Cash D. 2016a. Whole-Brain Ex-Vivo Imaging Of Demyelination In The Cuprizone Mouse With mcDESPOT And DTI Proc ISMRM 24:1317.

Wood TC, Simmons C, Hurley SA, Vernon AC, Torres J, Dell'Acqua F, Williams SCR, Cash D. 2016b. Whole-brain ex-vivo quantitative MRI of the cuprizone mouse. Peer J. 4:e2323v1. https://doi.org/10.7287/peerj.preprints.2323v1.

Zorrilla EP. 1997. Multiparous species present problems (and possibilities) to developmentalists. Dev Psychobiol. 30:141–150.